

Multi-Scalar-Singlet Extension of the Standard Model - the Case for Dark Matter and an Invisible Higgs Boson -

A. Drozd^a B. Grzadkowski José Wudka

^a*Institute of Theoretical Physics, University of Warsaw, Hoża 69, PL-00-681 Warsaw, Poland*

^b*Department of Physics, University of California, Riverside CA 92521-0413, USA*

E-mail: Aleksandra.Drozd@fuw.edu.pl, Bohdan.Grzadkowski@fuw.edu.pl,
Jose.Wudka@ucr.edu

ABSTRACT: We consider a simple extension of the Standard Model by the addition of N real scalar gauge singlets $\tilde{\varphi}$ that are candidates for Dark Matter. By collecting theoretical and experimental constraints we determine the space of allowed parameters of the model. The possibility of ameliorating the little hierarchy problem within the multisinglet model is discussed. The Spergel-Steinhardt solution of the Dark Matter density cusp problem is revisited. It is shown that fitting the recent CRESST-II data for Dark Matter nucleus scattering implies that the standard Higgs boson decays predominantly into pairs of Dark Matter scalars. In that case discovery of the Higgs boson at LHC and Tevatron is impossible. The most likely mass of the dark scalars is in the range $15 \text{ GeV} \lesssim m_{\tilde{\varphi}} \lesssim 50 \text{ GeV}$ with $BR(h \rightarrow \tilde{\varphi}\tilde{\varphi})$ up to 96%.

KEYWORDS: dark matter, gauge singlet scalars, Higgs boson decay

ARXIV EPRINT: [1112.2582](https://arxiv.org/abs/1112.2582)

Contents

1	Introduction	1
2	The Model	2
3	Stability and perturbative unitarity	3
4	Triviality	3
5	Fine-tuning in Higgs mass corrections	4
6	DM relic abundance	10
6.1	Cold Dark Matter	11
6.2	Feebly Interacting Dark Matter (FIDM)	13
7	Direct detection	15
8	Self-interacting DM	19
9	Summary and conclusions	22

1 Introduction

The evidence for dark matter (DM) has now become almost overwhelming [1], yet the standard model (SM) does not contain a viable DM candidate, which necessitates a modification of this model. The simplest possible such extension consists of introducing a real scalar field which is a gauge singlet. Many authors considered this singlet extension of the SM; the earliest publication we are aware of was by Veltman and Yndurain in [2] (though their motivation was different). The DM issue was first addressed in this context in [3] and [4] and then followed by other authors [5]-[15].

In this paper we will consider a generalization of this model by extending the DM sector to an unbroken (global) $O(N)$ model. We will derive relevant theoretical and experimental constraints on this model and determine range of allowed parameters. Since we demand the new singlets do not acquire a vacuum expectation value, the effects of the dark sector on precision observables is much suppressed, appearing only at the two (or higher) loop level. The only experimental constraints are then obtained from the requirement that the scalars are adequate candidates for DM. The theoretical constraints on the model are derived from vacuum stability, perturbativity, and triviality. In addition we will also determine the fine tuning conditions that ameliorate the little hierarchy problem by seeking model parameters that tame quadratically divergent contributions to the Higgs boson mass [16], [17] following strategies adopted in [18].

The model discussed below is also interesting in light of the DM signals recently announced by the CRESST-II collaboration [19]. We will see that, not only the most likely regions found by CRESST-II are consistent with the model, but in a region of parameter space where the SM Higgs decays invisibly into DM pairs. Such a Higgs boson would not be detected at either the Tevatron or LHC.

The paper is organized as follows. In Sec. 2 we introduce the model and formulate strategy adopted in this paper for its study. In Sec. 3 we review the vacuum stability and unitarity bounds that restrict the parameter space of the model, while in Sec. 4 the issue of triviality is addressed. Sec. 5 is devoted to a discussion of one- and leading two-loop corrections to the Higgs boson mass in the presence of extra singlets. In Sec. 6 the present Dark Matter abundance is investigated for the Cold Dark Matter (CDM) and Feebly Interacting Dark Matter (FIDM) scenarios. Sec. 7 shows results of constraining the model by results of direct searches of DM. In Sec. 8 we revisit the Spergel-Steinhardt hypothesis of self-interacting DM. Sec. 9 contains summary and conclusions.

2 The Model

We consider the SM of electroweak interactions extended by the addition of N scalars $\vec{\varphi}$ that are singlets under the SM gauge group $SU(3) \times SU(2) \times U(1)$, and transforming according to the fundamental representation of $O(N)$, under which all SM fields are singlets; for simplicity we assume that $O(N)$ is an exact symmetry of the model¹. With the intention of providing a Dark Matter (DM) candidate we impose an additional Z_2 symmetry, which is not spontaneously broken, and under which $\vec{\varphi}$ is odd: $\vec{\varphi} \rightarrow -\vec{\varphi}$ while all other fields are even². The most general, symmetric and renormalizable potential reads:

$$V(H, \vec{\varphi}) = -\mu_H^2 H^\dagger H + \lambda_H (H^\dagger H)^2 + \frac{1}{2} \mu_\varphi^2 \vec{\varphi}^2 + \frac{1}{4!} \lambda_\varphi (\vec{\varphi}^2)^2 + \lambda_x H^\dagger H \vec{\varphi}^2, \quad (2.1)$$

where H is the SM $SU(2)$ Higgs isodoublet. The Lagrangian density for the scalar sector is then given by:

$$L_{\text{scalar}} = \frac{1}{2} \partial_\mu \vec{\varphi} \partial^\mu \vec{\varphi} + D_\mu H^\dagger D^\mu H - V(H, \vec{\varphi}). \quad (2.2)$$

As usually the minimum of the potential breaks spontaneously electroweak symmetry via non-zero vacuum expectation value of the Higgs doublet $\langle H \rangle = (0, v/\sqrt{2})$, $v = 246$ GeV. Since we require the $O(N)$ symmetry (Z_2 for $N = 1$) to remain unbroken, we assume that $\mu_\varphi^2 > 0$, so $\langle \vec{\varphi} \rangle = 0$. Note that $\langle \vec{\varphi} \rangle = 0$ implies no mass-mixing between $\vec{\varphi}$ and H , therefore the existing collider limits on the Higgs properties are not modified. After the symmetry breaking the physical scalars have masses $m_h^2 = -\mu_H^2 + 3\lambda_H v^2 = 2\mu_H^2$ and $m_\varphi^2 = \mu_\varphi^2 + \lambda_x v^2$. Note that all components of $\vec{\varphi}$ have the same mass as the consequence of $O(N)$, this degeneracy can be removed by adding a generic mass term $(\mu_\varphi)_{ij} \varphi_i \varphi_j$ that only breaks $O(N)$ softly.

¹This condition could be relaxed without significantly altering the conclusions; the only consequence would be the presence of many more parameters of the model.

²For $N > 1$ this Z_2 symmetry is a consequence of $O(N)$ invariance.

The model then contains five unknown parameters: $m_h, m_\varphi, \lambda_x, \lambda_\varphi, N$. Our goal is to constrain the parameters taking into account available restrictions: theoretical (vacuum stability, unitarity/perturbativity, triviality of the scalar sector, Higgs mass correction fine-tuning) and experimental (DM relic abundance, direct detection experiments).

3 Stability and perturbative unitarity

In order to stabilize vacuum we will assume that the scalar potential (2.1) is (at tree level) bounded from below. This condition implies

$$\lambda_H, \lambda_\varphi > 0; \quad \lambda_x > -\sqrt{\frac{\lambda_\varphi \lambda_H}{6}} = -\frac{m_h}{2v} \sqrt{\frac{\lambda_\varphi}{3}}. \quad (3.1)$$

Tree-level unitarity constraints emerge from the SM condition for $V_L V_L$ scattering [20] and from the requirement that all possible scalar-scalar scattering amplitudes are consistent with unitarity of the S matrix [21]

$$m_h^2 < \frac{8\pi}{3} v^2, \quad \lambda_\varphi < 8\pi \quad \text{and} \quad |\lambda_x| < 4\pi. \quad (3.2)$$

Finally, the condition that the global $O(N)$ symmetry remains unbroken requires $\mu_\varphi^2 > 0$ which leads to the very useful inequality:

$$m_\varphi^2 > \lambda_x v^2; \quad (3.3)$$

a consequence is that light scalars ($m_\varphi \ll v$) must couple very weakly to the SM ($\lambda_x \ll 1$).

4 Triviality

The 'triviality bound' is a constraint on the SM generated by the requirement that under the renormalization group evolution the quartic coupling constant λ_H remains finite up to the UV cut-off scale Λ of the model; in other words, that the Higgs-boson Landau pole should be above Λ . This requirement implies conditions on the initial values of various running parameters of the model, and in particular on $\lambda_H(\mu = m_W)$; this, in turn, leads to an upper limit on the Higgs boson mass as a function of Λ .

In order to determine the location of the Landau pole as a function of the Higgs mass one has to solve the renormalization group evolution (RGE) equations for all of the running parameters of the model. We will be interested only in cutoff scales below 50 TeV, in which case the RGE of the gauge and top-quark Yukawa couplings can be safely neglected. Thus we only need to consider the evolution of $\lambda_H, \lambda_\varphi$ and λ_x as determined by

$$16\pi^2 \mu \frac{d\lambda_H}{d\mu} = \frac{3}{8}g_1^4 + \frac{9}{8}g_2^4 + \frac{3}{4}g_1^2 g_2^2 - 6y_t^4 + 24\lambda_H^2 + 12y_t^2 \lambda_H - 3g_1^2 \lambda_H - 9g_2^2 \lambda_H + 2N\lambda_x^2 \quad (4.1)$$

$$16\pi^2 \mu \frac{d\lambda_x}{d\mu} = \lambda_x \left(12\lambda_H + \lambda_\varphi + 8\lambda_x + 6y_t^2 - \frac{3}{2}g_1^2 - \frac{9}{2}g_2^2 \right) \quad (4.2)$$

$$16\pi^2 \mu \frac{d\lambda_\varphi}{d\mu} = 48\lambda_x^2 + \frac{1}{3}(8+N)\lambda_\varphi^2 \quad (4.3)$$

where g_1, g_2, g_3 are the gauge coupling for $U(1), SU(2), SU(3)$, respectively, and y_t is the top quark Yukawa coupling. Unique solutions could be obtained once the initial conditions

$$\lambda_H(\mu = m_W) = \lambda_{H0} \quad (4.4)$$

$$\lambda_x(\mu = m_W) = \lambda_{x0} \quad (4.5)$$

$$\lambda_\varphi(\mu = m_W) = \lambda_{\varphi0} \quad (4.6)$$

are specified.

For a given Λ we shall require that there is no pole in the evolution of scalar quartic coupling constants at energies below Λ . The region in the $(\Lambda, m_h = v\sqrt{2\lambda_{H0}})$ plane allowed by this constraint, depends on the initial parameters $\lambda_{x0}, \lambda_{\varphi0}$, and the number of scalars N . For each Λ the maximum allowed value of m_h constitutes the triviality bound on the Higgs mass. One might worry that each quartic coupling constant will have a different pole location, this, however, does not occur when $\lambda_{x0} \neq 0$ (as we assume), for then all the RGE equations are coupled and $\lambda_{H,\varphi,x}$ diverge at the same value of μ .

The triviality bound for m_h as a function of Λ is illustrated in Fig. 1. Note that the allowed region shrinks as λ_{x0} grows for fixed N , and as N increases for fixed λ_{x0} , lowering the upper bound on m_h in either case. This behavior is a direct consequence of the term $2N\lambda_x^2$ in (4.1): increasing N and/or λ_x amplifies the evolution of λ_H . For a given (Λ, m_h) and fixed $\lambda_{\varphi0}$ there is a range of λ_{x0} for which the Landau pole occurs above Λ , as shown in Fig. 3. Note the asymmetry of the allowed (inner) region, which is a consequence of the $8\lambda_x^2$ term in (4.2).

In Fig. 2 we show triviality limits for λ_φ as a function of Λ for the case $\lambda_{x0} = 0$ when the $\tilde{\varphi}$ evolution decouples from the SM.

5 Fine-tuning in Higgs mass corrections

If we assume that the SM is an effective theory valid at scales below the UV cutoff Λ , radiative corrections [22] shift the Higgs mass to a scale of order $\Lambda/\sqrt{4\pi}$. The existing bounds on the scale of new physics imply $\Lambda > O(\text{TeV})$, which is in conflict with a Higgs mass below 1 TeV range as required by the unitarity constraint [20]. A way of alleviating this conflict is to arrange cancellations to occur within the $O(\Lambda^2)$ contributions to m_h^2 . These cancellations can be obtained through a fine tuning of the parameters or through an extension of the SM together with an appropriate new symmetry (as is the case in supersymmetric models).

The first solution to this problem was proposed by Veltman [22] who observed that the 1-loop quadratic corrections to m_h would vanish if $m_h^2 + m_Z^2 + 2m_W^2 - 4m_t^2 = 0$, but this possibility is now experimentally disallowed. Here we shall follow a similar approach within the multi-singlet extension of the SM.

In pursuing this approach it is important to determine the possible effects generated by higher order radiative corrections. In a theory with many couplings λ_i the general form of leading higher-order contributions (those containing the highest power of $\log(\Lambda)$) to the

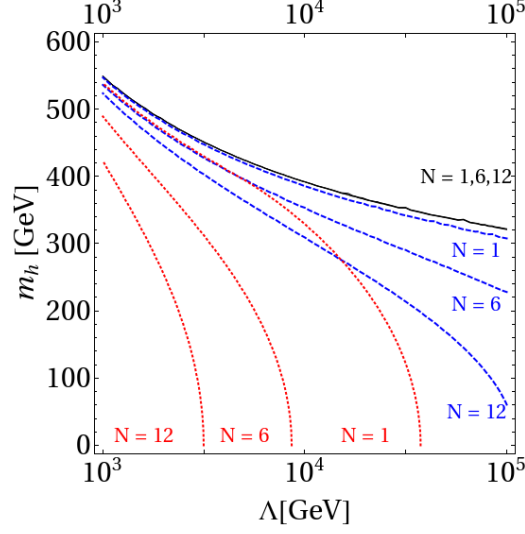


Figure 1. The triviality upper bound on the Higgs mass as a function of the cut-off Λ for $\lambda_\varphi(m_W) = 0.1$, for $\lambda_{x0} = 0.1, 1, 2$ (black, blue and red curves, respectively) and $N = 1, 6, 12$ (starting with the uppermost curve); the region above each curve is excluded by the triviality constraint for the corresponding set of parameters. For $\lambda_{x0} = 0.1$ non-standard effects are so small that upper boundaries for $N = 1, 6$ and 12 are indistinguishable from the SM, accordingly the black curves are nearly identical to the bound derived within the SM.

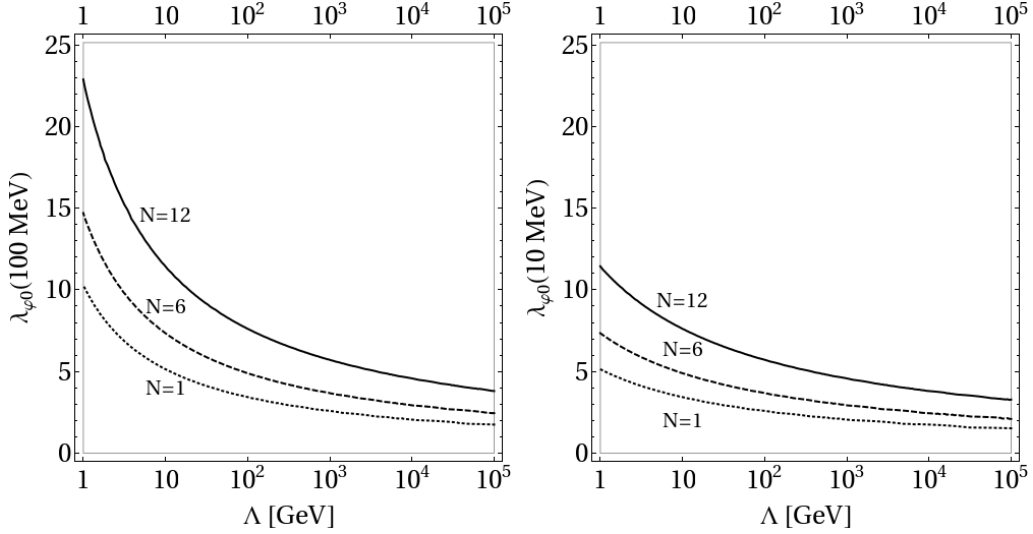


Figure 2. Maximum $\lambda_{\varphi0}$ allowed by the triviality condition as a function of Λ for $N = 1, 6, 12$ and $\lambda_{x0} = 0$. The right (left) panel is for initial conditions provided at a 10 MeV (100 MeV)

quadratically divergent contributions to m_h^2 at $n + 1$ loops take the form [23]

$$\delta m_h^2 = \Lambda^2 \sum_{n=0}^{\infty} f_n(\lambda_i) \left[\log \left(\frac{\Lambda}{\mu} \right) \right]^n \quad (5.1)$$

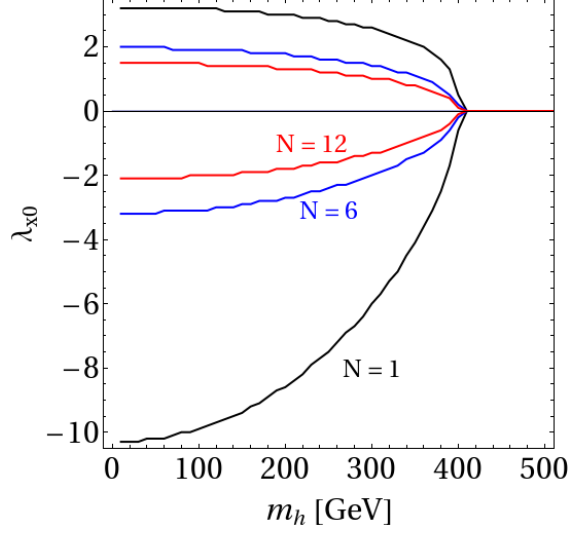


Figure 3. Maximum and minimum λ_{x0} allowed by the triviality bound for $\Lambda = 10$ TeV, $\lambda_{\varphi 0} = 0.1$ and $N = 1, 6, 12$.

where μ is the renormalization scale and the coefficients f_n satisfy

$$(n+1)f_{n+1} = \mu \frac{\partial}{\partial \mu} f_n = \beta_i \frac{\partial}{\partial \lambda_i} f_n. \quad (5.2)$$

Thus in order to determine the two-loop leading logarithmic corrections to the Higgs mass one needs the one-loop corrections and the first order beta functions (for generic results and applications to the single scalar case see [24]). The results for N -singlet model read:

$$\begin{aligned} \delta m_{h1-loop}^2 = & \frac{\Lambda^2}{16\pi^2} \left(12\lambda_H + 2N\lambda_x - 12y_t^2 + \frac{3}{2}g_1^2 + \frac{9}{2}g_2^2 \right) \\ & - \frac{1}{16\pi^2} \left[6\lambda_H m_h^2 \log \left(\frac{m_h^2 + \Lambda^2}{m_h^2} \right) + 2\lambda_x m_\varphi^2 \log \left(\frac{m_\varphi^2 + \Lambda^2}{m_\varphi^2} \right) \right] \end{aligned} \quad (5.3)$$

$$\begin{aligned} \delta m_{h2-loops}^2 = & \frac{\Lambda^2}{(16\pi^2)^2} \log \left(\frac{\Lambda}{\mu} \right) [25g_1^4 + 9g_1^2g_2^2 - 15g_2^4 + 34g_1^2y_t^2 + 54g_2^2y_t^2 \\ & + 192g_3^2y_t^2 - 180y_t^4\lambda_H - 36g_1^2 - 108g_2^2\lambda_H + 144y_t^2\lambda_H + 288\lambda_H^2 \\ & - 3Ng_1^2\lambda_x - 9Ng_2^2\lambda_x + 12Ny_t^2\lambda_x + 24N\lambda_H\lambda_x + 40N\lambda_x^2 + 2N\lambda_x\lambda_\varphi] \end{aligned} \quad (5.4)$$

the logarithmic terms ($\propto m_\varphi^2 \log \Lambda$) in the one-loop correction were kept since they are relevant in the range $m_h \ll m_\varphi \lesssim \Lambda$; terms $\propto m_h^2 \log \Lambda$ are always numerically negligible and are included for completeness. For the numerical results the renormalization scale was chosen to be the vacuum expectation value of the Higgs field, $\mu = 246$ GeV. The SM result can be recovered in the limit $\lambda_x = \lambda_\varphi = 0$.

We implement the fine tuning condition in a standard manner [18] by requiring

$$\left| \frac{\delta m_h^2}{m_h^2} \right| \equiv \left| \frac{\delta m_{h1-loop}^2 + \delta m_{h2-loops}^2}{m_h^2} \right| \leq \Delta_h \quad (5.5)$$

and determine the region in the (Λ, m_h) plane where this is obeyed for a given choice of the fine tuning parameter Δ_h . Specifically, for each choice of (Λ, m_h) with fixed N and λ_x we check if there exist m_φ and λ_φ such that condition (5.5) is satisfied; the results are presented in Figs. 4 and 5.

It is worth noting that the two-loop $\vec{\varphi}$ corrections to m_h (5.4) grow as $\lambda_x/(16\pi^2) \ln(\Lambda/\mu)$ relative to the one-loop contributions (5.3). Perturbative consistency then requires this factor to be ≤ 1 , which translates into a maximal cutoff Λ_{\max} beyond which perturbation theory is no valid:

$$\Lambda \lesssim \Lambda_{\max} = \mu e^{4\pi^2/(5\lambda_x)} \quad (5.6)$$

Therefore the regions of large Λ in Figs. 4 and 5 should be considered with a certain caution (that should increase with λ_x). The range of Λ is extended up to 10^6 GeV only for the purpose of the SM ($\lambda_x = 0$) and small λ_x cases ($\lambda_x \lesssim 0.95$ for $\mu = 246$ GeV).

We now consider the regions in the (Λ, m_h) excluded by the triviality and fine tuning constraints, first for $\lambda_x \geq 0$ and then for $\lambda_x < 0$.

$\lambda_x \geq 0$. As one can see in Fig. 4, the fine-tuning condition (5.5) defines a region in the (Λ, m_h) plane with a characteristic funnel-shaped boundary (bounded, for various values of λ_x , by the solid lines shown in the figure). Given the experimental bounds [25] on m_h , $115 \text{ GeV} < m_h < 141 \text{ GeV}$, we see that as λ_x or N grows, the lower branch of the funnel allows larger regions of Λ for fixed Δ , or smaller values of Δ_h for fixed Λ ; in contrast the upper branch of the funnel allows smaller regions of Λ for fixed Δ_h , or larger values of Δ_h for fixed Λ . As a result the combined effect is complicated, for example the region allowed by (5.5) and the experimental limits on m_h shrinks as λ_x goes from 1.25 to 2 when $N = 1$, and as λ_x goes from 0.5 to 1 for $N = 3$. For fixed λ_x and N the allowed range of Λ shrinks as Δ_h becomes smaller.

Several comments are in order here. For the SM ($\lambda_x = 0$) there is a disallowed region for Λ between $1 - 10 \text{ TeV}$ and $\sim 10^3 \text{ TeV}$; this region shrinks as Δ grows. For instance, if $\Lambda \sim 10^4 \text{ GeV}$ then the present limits on the Higgs boson mass, can be accommodated only for large fine tuning: $\Delta_h > 100$. In order to have $\Delta_h < 100$ a modification of the SM must be introduced, or low ($\sim 1 \text{ TeV}$) or very high $\gtrsim 10^3 \text{ TeV}$ values of Λ must be assumed.

Note that for each point (Λ, m_h) below the SM ($\lambda_x = 0$) upper branch there exist λ_x such, that the point is allowed. Therefore in the model we discuss here, for a fixed cutoff Λ , much smaller Higgs-boson masses are allowed. In particular the range of $115 \text{ GeV} < m_h < 141 \text{ GeV}$ could be easily accommodated with a cutoff much larger than the SM one.

Let's concentrate on the cutoff $\Lambda = 10^4 \text{ GeV}$. As it is seen from the left panels in Fig. 4 for such Λ , in order to have the range of presently allowed Higgs masses $115 \text{ GeV} < m_h < 141 \text{ GeV}$ within the region of fine tuning $\delta m_h^2/m_h^2$ below 10, one needs λ_x of the order of $1.2 - 1.3$ and $0.5 - 0.6$ for $N = 1$ and $N = 3$, respectively. However, if we relax the fine tuning condition so that $\delta m_h^2/m_h^2 < 100$ (see the right panels of Fig. 4) then, as expected, lower λ_x is sufficient; $\lambda_x \simeq 1$ for $115 \text{ GeV} < m_h < 130 \text{ GeV}$ and $\lambda_x \simeq 0.5$ for $130 \text{ GeV} < m_h < 141 \text{ GeV}$, for $N = 1$. If $N = 3$, then $\lambda_x \simeq 0.5$ is large enough to bring the whole m_h range into the region of the fine tuning $\delta m_h^2/m_h^2 < 100$. In general, $\lambda_x = O(1)$ is needed to ameliorate the SM fine tuning.

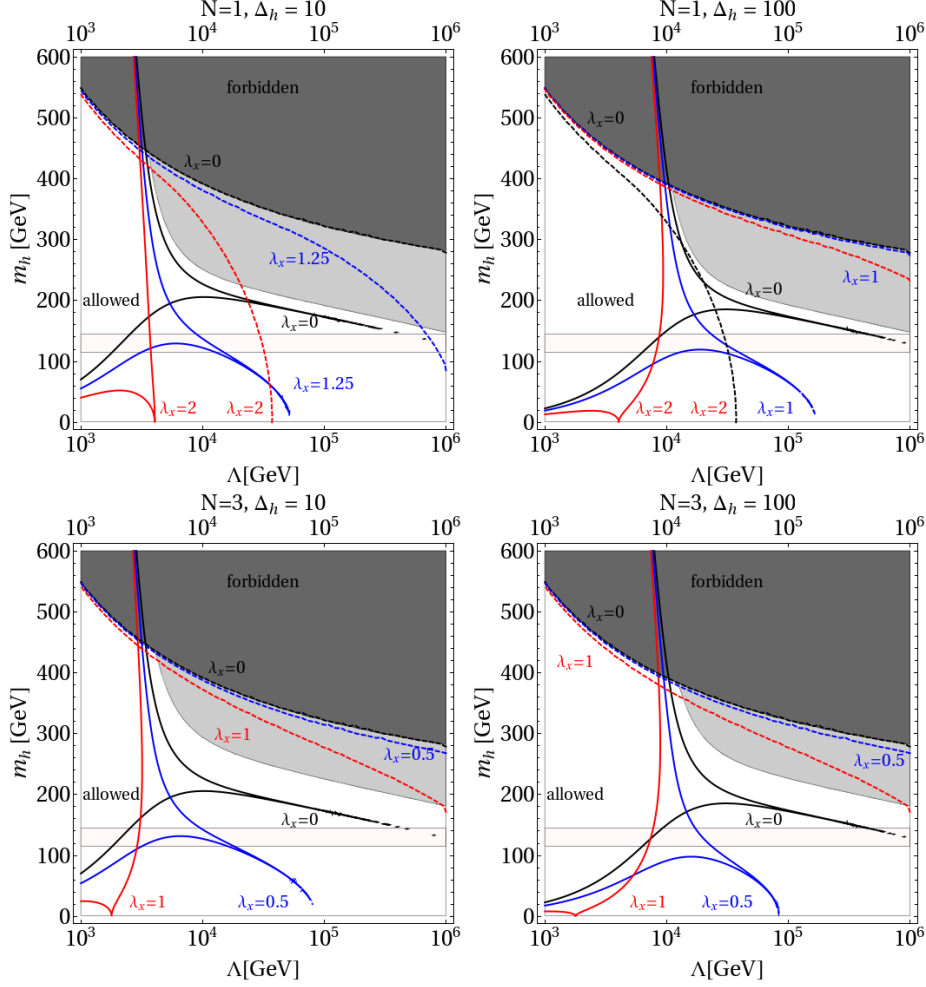


Figure 4. Constraints on m_h and Λ for $\Delta_h = 1, 10$ and $N = 1, 3$. The horizontal band shows the presently allowed range for the Higgs-boson mass [25]: $115 \text{ GeV} < m_h < 141 \text{ GeV}$. Dashed curves correspond to the triviality limits for the SM ($\lambda_x = 0$, dashed black curve) and singlet extensions for several values of λ_x (dashed blue and red curves); regions below the curves are allowed by this constraint. The solid lines correspond to the two-loop fine-tuning constraint for the SM ($\lambda_x = 0$, solid black) and singlet extensions for several values of λ_x (solid red and blue curves), the regions to the left of the corresponding funnels are allowed by this constraint. Every point inside the dark (light) gray region is forbidden by the triviality (fine tuning) condition for any value of λ_x . For every allowed point outside the dark gray and gray regions there exist $|\lambda_x| < 8\pi$, $10 \text{ GeV} < m_\varphi < 10^4 \text{ GeV}$ and $0 < \lambda_\varphi < 2$ such that (5.5) is fulfilled.

On the other hand, one should remember that for each choice of m_φ , λ_x is restricted from above by the condition (3.3), therefore if $0.5 < \lambda_x < 1.5$, then the corresponding $\vec{\varphi}$ mass must be in the range $174 \text{ GeV} < m_\varphi < 301 \text{ GeV}$. Alternatively, if we require $m_\varphi = 15 - 60 \text{ GeV}$ (the range relevant for direct DM detection, see Sec. 7) then $0.06 < \lambda_x < 0.24$; as seen from Fig. 4 such low $\vec{\varphi}$ masses are inconsistent with $\Delta_h = 100$, $\Lambda = 10^4 \text{ GeV}$ and $N = 1$ or 3 . In order to allow for that low mass, either larger N , $\Delta_h > 100$ or lower cutoff Λ would be necessary.

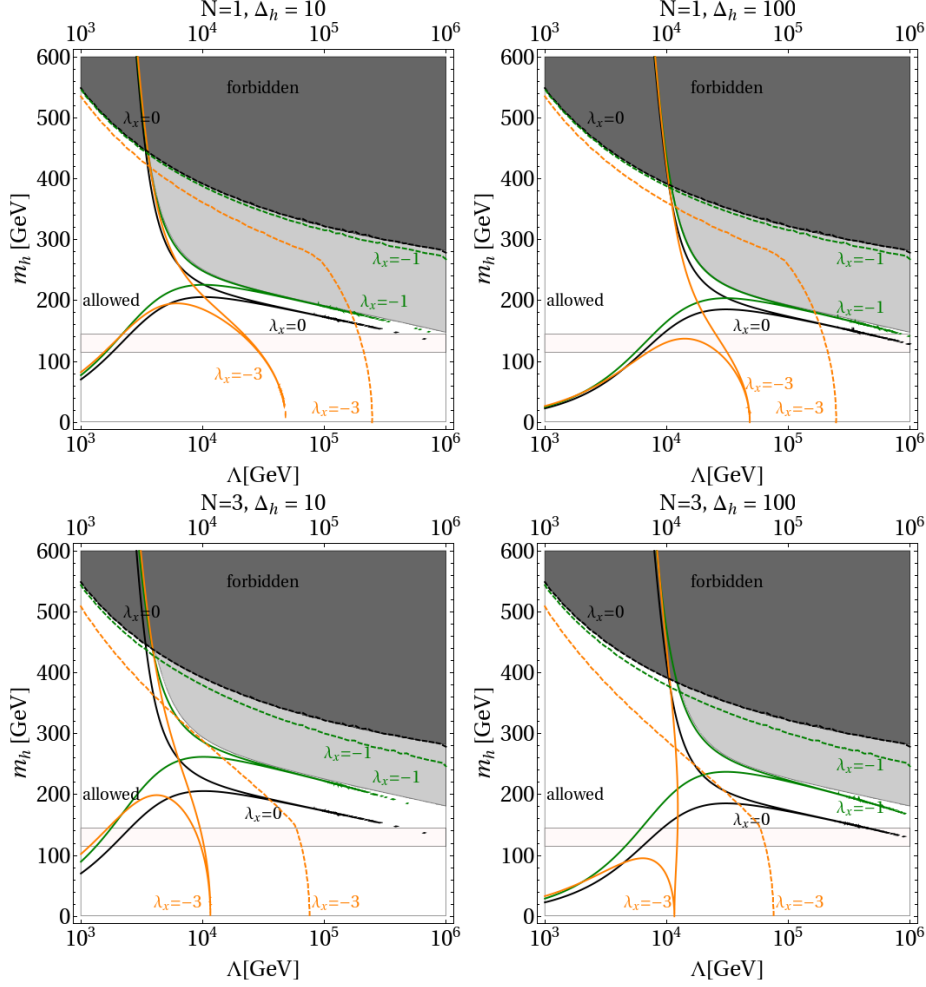


Figure 5. Similar as Fig. 4 for negative λ_x .

It is worth noting that for large m_h ($m_h \gtrsim 310$ GeV) the SM contribution to the quadratic divergence is dominated by the Higgs boson, therefore in order to enlarge the allowed region the extra contribution from $\tilde{\varphi}$ in the loop should be of the opposite sign (corresponding to $\lambda_x < 0$).

$\lambda_x < 0$. In this case the limit (3.3) provides no restriction, on the other hand the vacuum stability condition (3.1) becomes important. This constraint allows $|\lambda_x| > 1$ but only for $m_h > 170$ GeV due to the unitarity limit (3.2); saturating this limit by taking $\lambda_\varphi = 8\pi$ requires $|\lambda_x| < 0.65 - 0.85$ for $110 \text{ GeV} < m_h < 141 \text{ GeV}$. In this range the allowed values of Λ are more restricted when the singlets are included than for the SM, this is because for $\lambda_x < 0$ the 1-loop $\tilde{\varphi}$ -contribution to δm_h^2 is of the same sign as the top-quark one, therefore for small λ_x funnels are shifted towards larger values of m_h , as needed by (5.5) in order to compensate the top and $\tilde{\varphi}$ effects; as λ_x increases the funnels move downwards as a consequence of the growing 2-loop contributions to $\delta m_h^2_{2\text{-loops}}$.

The dashed curves in Figs. 4 and 5 give the triviality limits on m_h for various values

of λ_x (see also Fig. 1). As seen from the figures, this constraint is not important for $115 \text{ GeV} < m_h < 141 \text{ GeV}$.

Summarizing this section, one can say, that for $0 < \lambda_x \lesssim 1$ the model allows to shift the UV cutoff up to $\Lambda \lesssim 10^4 \text{ GeV}$ keeping the Higgs-boson mass within the experimentally allowed range $115 \text{ GeV} < m_h < 141 \text{ GeV}$. The case $\lambda_x < 0$ is disfavored, as the cutoff in this case appears to be lower than in the SM as long as we stay within the range of parameters allowed by perturbative expansion.

6 DM relic abundance

The singlet $\vec{\varphi}$, being odd under the Z_2 symmetry, is stable, and therefore a dark matter candidate, in which case the parameters of the theory should also lead to the DM abundance consistent with the WMAP observations, $\Omega_{\text{DM}}^{(\text{exp})} = 0.110 \pm 0.018$ (3σ) [26]. In order to gauge the consequences of this constraint on our model we first calculate the relic DM abundance by solving the appropriate Boltzmann equation. Considering first the single component ($N = 1$) case, we have [27]:

$$\frac{df}{dT} = \frac{\langle \sigma v \rangle}{K} (f^2 - f_{EQ}^2), \quad K(T) = \sqrt{\frac{4\pi^3 g_*(T)}{45 m_{Pl}^2}}, \quad f_{EQ}(T) = \int \frac{d^3 p}{(2\pi)^3} \frac{1}{\exp(E/T) \pm 1} \quad (6.1)$$

where $f \equiv n/T^3$, n is the particle number density of the DM candidate (in our case the singlet), $f_{EQ}(T)$ is the equilibrium distribution, $g_*(T)$ is the number of relativistic degrees of freedom at temperature T , m_{Pl} is the Planck mass and $\langle \sigma v \rangle$ is the thermally-averaged cross section for $DM + DM \rightarrow SM + SM$ annihilation processes ([28], [10]):

$$\langle \sigma v \rangle = \frac{x}{16 m_\varphi^5 K_2^2(x)} \int_{4m_\varphi^2}^{\infty} ds K_1 \left(\frac{\sqrt{s}}{T} \right) \sqrt{s - 4m_\varphi^2} \hat{\sigma}(s), \quad (6.2)$$

$$\hat{\sigma}(s) = 2 \sqrt{s(s - 4m_\varphi^2)} \sigma(s) \quad (6.3)$$

where $x = m_\varphi/T$, $K_{1,2}(x)$ are the modified Bessel functions, and $\sigma(s)$ is the $DM + DM \rightarrow SM + SM$ annihilation cross section normalized in the standard manner. In analytical estimates is useful to note that $\langle \sigma v \rangle \sim \hat{\sigma}(4m_\varphi^2)/4m_\varphi^2$ for non-relativistic DM; however we do not use this approximation in the numerical results shown below.

In the case of N -singlet scalar DM candidates with $O(N)$ symmetry, all components contribute equally to the relic abundance, just like a single field with N degrees of freedom. Therefore the total abundance equals

$$\Omega_{\text{DM}}^N = \sum_i \Omega_{\text{DM}}^i = N \Omega_{\text{DM}}^1 \quad (6.4)$$

where Ω_{DM}^i is the dark matter relic density from the i -th scalar field. By virtue of the $O(N)$ symmetry it is sufficient to consider the Boltzmann equation for one of the components of $\vec{\varphi}$.

In the following we will discuss two different limiting cases for the Boltzmann equation: Cold Dark Matter (CDM) and Feebly Interacting Dark Matter (FIDM). We do not consider

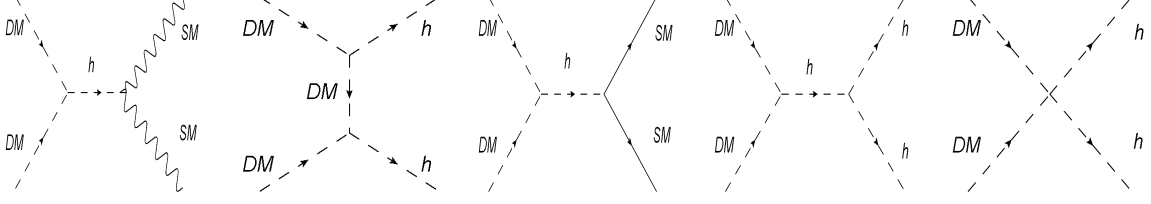


Figure 6. Feynman diagrams illustrating $\bar{\varphi}\varphi$ annihilation into SM particles.

the hot dark matter solution, since it is inconsistent with structure formation at the galaxy scale, see e.g. [29].

The diagrams contributing to $\bar{\varphi}\varphi$ annihilation into SM particles are shown in Fig. 6. The corresponding cross sections (for $N = 1$) are available in the literature (e.g. [5] and [10]); we have verified the results of [10]:

$$\begin{aligned}\hat{\sigma}_{WW}(s) &= \frac{\lambda_x^2}{2\pi} \sqrt{1 - \frac{4M_W^2}{s}} \frac{s^2}{(s - m_h^2)^2 + m_h^2 \Gamma_h^2} \left(\frac{12M_W^4}{s^2} - \frac{4M_W^2}{s} + 1 \right) \\ \hat{\sigma}_{ZZ}(s) &= \frac{\lambda_x^2}{4\pi} \sqrt{1 - \frac{4M_Z^2}{s}} \frac{s^2}{(s - m_h^2)^2 + m_h^2 \Gamma_h^2} \left(\frac{12M_Z^4}{s^2} - \frac{4M_Z^2}{s} + 1 \right) \\ \hat{\sigma}_{\bar{f}f}(s) &= \frac{\lambda_x^2}{\pi} \left(\sqrt{1 - \frac{4m_f^2}{s}} \right)^3 \frac{m_f^2 s}{(s - m_h^2)^2 + m_h^2 \Gamma_h^2} \\ \hat{\sigma}_{hh}(s) &= \frac{\lambda_x^2}{4\pi} \sqrt{1 - \frac{4m_h^2}{s}} \left(\frac{(s + 2m_h^2)^2}{(s - m_h^2)^2} + \frac{32v^4 \lambda_x^2}{(s - 2m_h^2)^2} \left(\frac{1}{1 - \xi^2} + F(\xi) \right) - \frac{16v^2 \lambda_x (s + 2m_h^2)}{(s - 2m_h^2)(s - m_h^2)} F(\xi) \right)\end{aligned}$$

where $F(\xi) = \text{ArcTanh}(\xi)/\xi$, $\xi = \sqrt{(s - 4m_h^2)(s - 4m_\varphi^2)}/(s - 2m_h^2)$. The total cross section is then

$$\hat{\sigma}(s) = \hat{\sigma}_{WW}(s) + \hat{\sigma}_{ZZ}(s) + \sum_f \hat{\sigma}_{\bar{f}f}(s) + \hat{\sigma}_{hh}(s) \quad (6.6)$$

where the sum runs over all fermions f .

When $N > 1$ one has to modify the Higgs width as it can decay into N possible $\varphi_i \varphi_i$ final states:

$$\Gamma_h = \Gamma_{h \rightarrow SM} + \Gamma_{h \rightarrow \varphi\varphi} \quad (6.7)$$

$$\Gamma_{h \rightarrow \varphi\varphi} = \frac{Nv^2 \lambda_x^2}{8\pi m_h^2} \sqrt{m_h^2 - 4m_\varphi^2} \theta_H(m_h - 2m_\varphi) \quad (6.8)$$

where θ_H is the Heaviside step function.

6.1 Cold Dark Matter

In the CDM approximation the solution to the Boltzmann equation for the $O(N)$ model yields the relic density [27]

$$\Omega_{\text{DM}}^N h^2 = N \frac{\rho_{\text{DM}}^1}{\rho_{\text{crit}}} = 1.06 \times 10^9 \frac{N x_f}{\sqrt{g_*} m_{Pl} \langle \sigma v \rangle} \frac{1}{\text{GeV}} \quad (6.9)$$

where $x_f \equiv m_\varphi/T_f$, and T_f is the freeze-out temperature given in the first approximation by

$$x_f = \log \left(0.038 \frac{\langle \sigma v \rangle m_{Pl} m_\varphi}{\sqrt{g_*(T_f)} x_f} \right) \quad (6.10)$$

where $\langle \sigma v \rangle$ is the thermally averaged cross section for $\varphi_1 + \varphi_1 \rightarrow SM + SM$. Note that the N -dependence of x_f enters through the Higgs width (6.7) contained in $\langle \sigma v \rangle$; this weak dependence is further softened by the log function in (6.10). Therefore it is reasonable to neglect the N dependence in x_f (at least in the parameter range where the perturbative expansion is valid). Note also that in the case where the t - and u -channel annihilation diagrams with $\vec{\varphi}$ exchange can be neglected (e.g. when $m_\varphi \gg m_h$ and/or if $\lambda_x \ll 1$), the abundance depends only on the combination $N\lambda_x^2$.

For a given choice of N and (m_h, m_φ) we will look for λ_x such that the constraint $\Omega_{DM}^{(exp)} = 0.110 \pm 0.018$ is satisfied:

$$0.092 < \Omega_{DM}^N < 0.128. \quad (6.11)$$

Even though (6.9) often leads to accurate results for the abundance, in deriving our numerical results we used micrOMEGAs [30] – a code dedicated for calculation of DM properties. Our results are presented in Fig. 7, where we have also included the restrictions derived from the consistency condition (3.3) and the vacuum stability constraint (3.1), which are relevant for $\lambda_x > 0$ and $\lambda_x < 0$, respectively.

To discuss solutions for λ_x shown in Fig. 7 it is useful to consider the following regions for (m_h, m_φ) :

- $m_\varphi \gtrsim m_h$

In this region m_φ is large, so the t - and u -channel annihilation diagrams with $\vec{\varphi}$ exchange can be neglected. In this approximation $\langle \sigma v \rangle$ depends on λ_x^2 , so there is no difference between left and right panels in Fig. 7. For $\lambda_x > 0$, the constraint (6.11) is consistent with (3.3) in this mass range, however for negative λ_x (3.1) requires $m_\varphi \lesssim 1$ TeV.

For $\lambda_x > 0$ the range of very heavy scalar masses $m_\varphi \sim 1 - 8$ TeV, corresponds to $\lambda_x \sim 1 - 10$, which though large, remains below the unitarity and consistency limits. In this region of parameter space the singlets provide a substantial contribution to δm_h^2 that can ameliorate the hierarchy problem (see Fig. 4), and was utilized for this purpose in [16].

- $m_h/2 \lesssim m_\varphi \lesssim m_h$

In this mass range the interference between s - and t - and u -channel annihilation diagrams is relevant, so some differences between negative and positive λ_x solutions are visible. For large N and $\lambda_x > 0$ a small region is excluded by (3.3).

- $m_\varphi \sim m_h/2$

In the vicinity of the resonance, the annihilation cross section is strongly enhanced, so that (6.11) can be satisfied only for small $|\lambda_x|$.

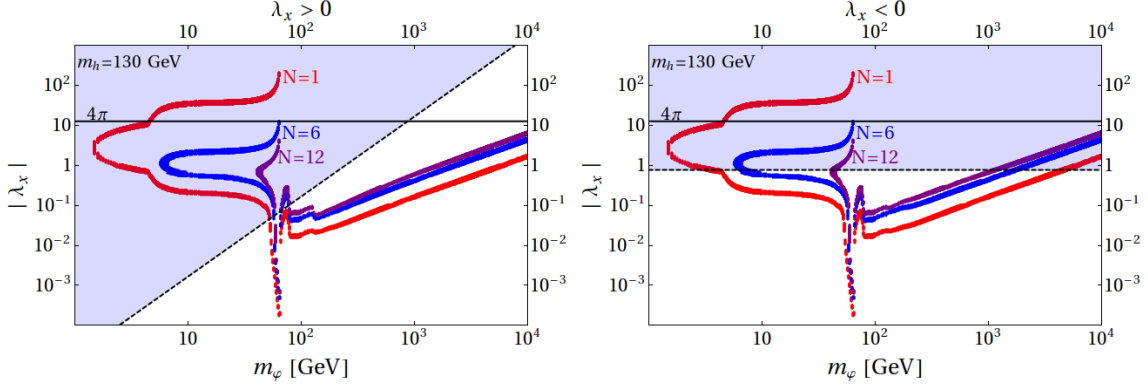


Figure 7. The coupling λ_x as a function of m_φ obtained from the requirement (6.11); for a the Higgs $m_h = 130$ GeV, $N = 1, 6$ and 12 (red, blue and purple bands respectively), and $\lambda_x > 0$ (left panel) or $\lambda_x < 0$ (right panel). The blue areas in the left and right panels correspond to the regions disallowed by the consistency condition (3.3) and stability constraint (3.1) for $\lambda_\varphi = 8\pi$, respectively. The thick black lines show the unitarity limit (3.2) saturated by $|\lambda_x| = 4\pi$.

- $m_\varphi \lesssim m_h/2$

In this case the process $\varphi\varphi \rightarrow hh$ is kinematically forbidden, so only the s -channel Higgs exchange graphs with no Higgs-bosons in the final state contribute; as a consequence $\langle\sigma v\rangle \propto \lambda_x^2$ and there is no difference between left and right panels Fig. 7 for this mass range. For $\lambda_x > 0$ this mass region is excluded by (3.3), while for $\lambda_x < 0$ values of m_φ below $m_h/2$ are allowed depending on N .

For scalar masses below ~ 1 GeV there are no CDM solutions.

6.2 Feebly Interacting Dark Matter (FIDM)

In order to thermalize with the SM particles, any other species of density n must have a thermalization rate $\Gamma = n \langle\sigma v\rangle$ larger than the expansion rate H . For relativistic singlets one can estimate $\Gamma \sim \lambda_x^2 T / (8\pi)$ while $H \sim T^2 / m_{Pl}$, therefore equilibrium prevails for $T < T_{EQ}$ where

$$T_{EQ} \sim \frac{m_{Pl} \lambda_x^2}{8\pi}. \quad (6.12)$$

If λ_x is very small ($\sim 10^{-9}$) the species of DM being considered here does not equilibrium until very late times $T_{EQ} \sim 1$ GeV; for $\lambda_x \lesssim 7 \times 10^{-16}$, $T_{EQ} < 2.7^\circ K$ and the singlets would not have equilibrated before the present epoch.

In the following we will consider the case of feebly interacting DM (FIDM). We will assume that the DM number density f was negligible at the Big Bang: $\lim_{T \rightarrow \infty} f(T) = 0$ and solve the Boltzmann equation for $N = 1$ (6.1) with this initial condition³; this then determines the relic abundance:

$$\Omega_{DM}^N h^2 = N \frac{m_\varphi n}{\rho_{crit}} = \frac{N m_\varphi T_\gamma^3}{\rho_{crit}} f \quad (6.13)$$

³In practice, the Boltzmann equation (6.1) simplifies for this initial condition since the f^2 term on the right-hand side can be dropped: the DM particles do not annihilate when $\lim_{T \rightarrow \infty} f(T) = 0$.

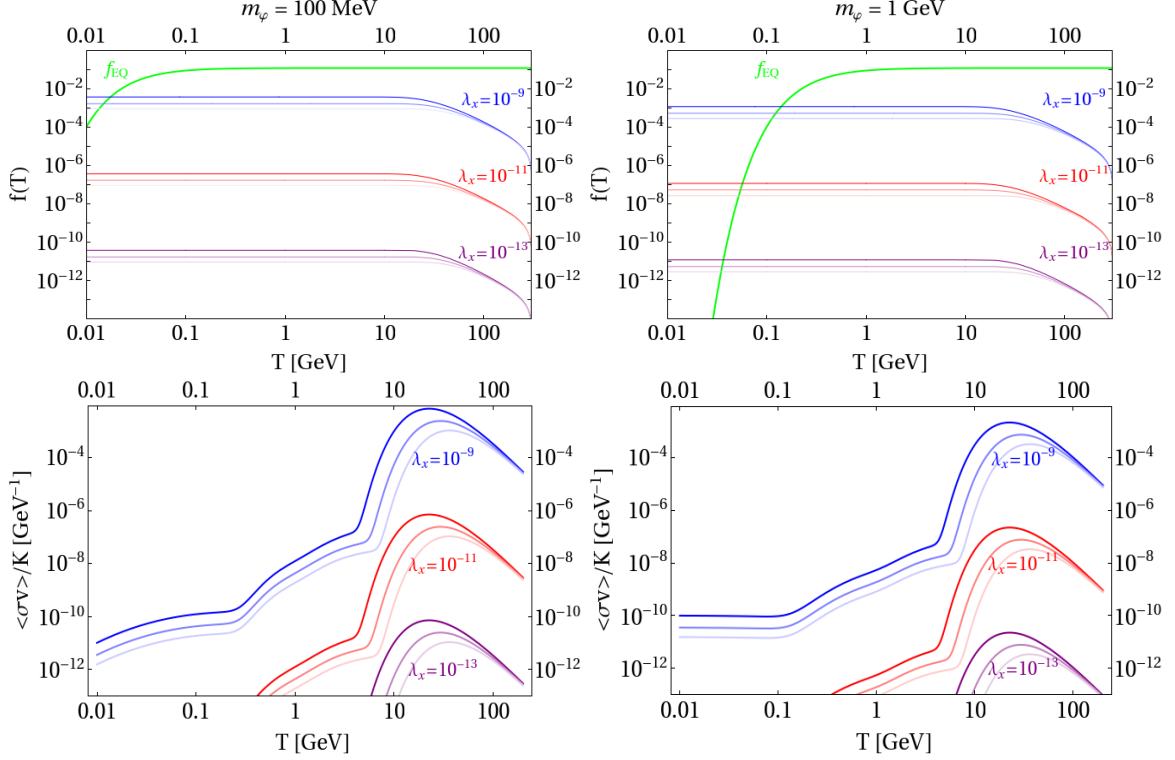


Figure 8. Top panels: FIDM solutions to the Boltzmann equation (6.1) with boundary condition $f(T = \infty) = 0$, $N = 1$ for two values of m_φ and $m_h = 100$ GeV (thin lines), 130 GeV (medium lines), 160 GeV (thick lines) and $|\lambda_x| = 10^{-13}$ (bottom curves), 10^{-11} (middle curves), 10^{-9} (top curves). The curve labeled f_{EQ} corresponds to the equilibrium distribution. Bottom panels: corresponding curves for $\langle\sigma v\rangle/K$ in (6.1).

where T_γ is the present photon temperature, and ρ_{crit} is the critical density. Following this procedure it should be remembered that the electroweak phase transition occurs at $T_{EW} \simeq 300$ GeV. Above this temperature, the only tree level contribution to the annihilation cross section comes from the $\lambda_x H^\dagger H \tilde{\varphi}^2$ coupling, therefore

$$\hat{\sigma}_{>300} = \frac{\lambda_x^2}{4\pi} \sqrt{1 - \frac{4m_h^2}{s}} \quad (6.14)$$

The case of FIDM was discussed first by McDonald in [31] and more recently also in [12] and [14]. In [31] the contribution from the process $\tilde{\varphi}\tilde{\varphi} \leftrightarrow H$ was included as a separate, and dominant, term in the Boltzmann equation. Here we obtain similar results following a different approach, where the presence of a non-zero width Γ_H (see (6.5)) accounts for the creation and decay contributions of the Higgs boson. In other words, to avoid possibility of double counting we assume that the thermal generation of scalars is included in the processes $DM + DM \leftrightarrow h \leftrightarrow SM + SM$.

The solutions of (6.1) for parameters relevant for insuring (6.11) are presented in top panels of Fig.8. As seen from this figure, if $\lambda_x \sim 10^{-9}$ the scalars will be in equilibrium with the SM only for $T \lesssim 100$ MeV in agreement with the estimate (6.12); for smaller

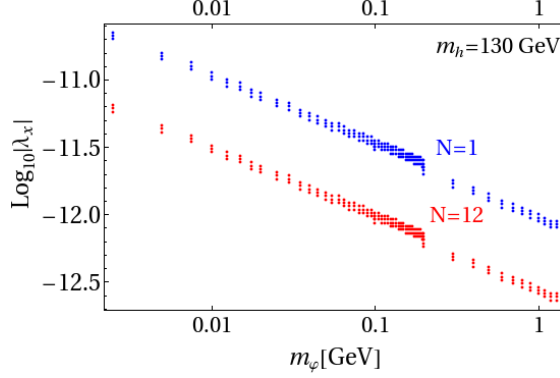


Figure 9. Solutions to the Boltzmann equation for FIDM, for $N = 1, 12$ scalars and $m_h = 130$ GeV.

λ_x equilibrium is reached only for even lower temperatures. In order to understand the behavior of the solutions for f we plot in the bottom panels of Fig. 8 the factor $\langle \sigma v \rangle / K$ appearing in (6.1) as a function of T . We see that $\langle \sigma v \rangle / K$ reaches its maximum for $T \sim 20 - 30$ GeV, and is strongly suppressed for $T \lesssim 10$ GeV. Because of this f becomes T -independent for $T \lesssim 20 - 30$ GeV, as observed in the top panels of the figure.

In the case of non-equilibrium solutions of the Boltzmann equation, (6.11) is satisfied only if $\lambda_x \ll 1$. For these small couplings we have $\langle \sigma v \rangle \propto \lambda_x^2$ up to small corrections, in addition the term $\propto f^2$ on the right-hand side of (6.1) is subdominant, so that to a good approximation $f \propto \lambda_x^2$. It then follows that for FIDM the relic density depends on the DM parameters in the combination $\Omega_{\text{DM}}^{(\text{exp})} \sim N m_\phi \lambda_x^2$; this behavior is indeed observed in Fig. 9. In particular DM masses above 1 GeV requires $\lambda_x < 10^{-13}$.

If the scalar masses are \sim MeV and $\lambda_x > 0$ then (3.3) requires $\lambda_x \ll 1$, for example $\lambda_x < 1.65 \times 10^{-7}$ and $\lambda_x < 1.65 \times 10^{-5}$ for $m_\phi = 100$ MeV and $m_\phi = 1$ GeV respectively. Note also that from Fig. 7 we conclude that there is no CDM solutions for $\lambda_x > 0$ and $m_\phi < 70$ GeV; for smaller masses, λ_x is also very small and the situation reverts to the FIDM scenario. One should however remember that solutions with $\lambda_x < 0$ are also possible; in this case Fig. 7 implies there are no CDM solutions for $m_\phi \lesssim 2$ GeV, then again the only solution is the FIDM shown in Fig. 9.

7 Direct detection

In this section we discuss constraints imposed on the model by searches for direct signals of DM particles scattering off nuclei. Even though the results of many experiments are available, here we will concentrate on the constraints obtained by the XENON100 experiment [32] as they impose strongest limits on DM - nucleon scattering cross-section $\sigma_{\text{DM-N}}$ in the mass range of our interest; at the end of this section we also comment on the recent results for the CRESST-II experiment [19].

The relevant scattering amplitude is described by the Feynman diagram in Fig. 10; the

corresponding cross section is

$$\sigma_{\text{DM-N}} = \frac{1}{\pi} \frac{\lambda_x^2 m_n^2 \left(\sum_q f_q^N \right)^2}{m_h^4 m_\varphi^2} \quad (7.1)$$

where the sum runs over all quark flavors q , m_n is the nucleon mass and f_q^N are the nucleon form factors as defined in [30].

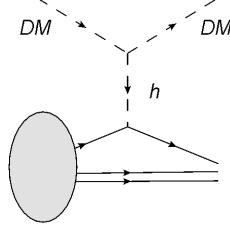


Figure 10. The Feynman diagram for the elastic scattering of $\tilde{\varphi}$ off a nucleon.

In Fig. 11 we show the regions in the (m_φ, m_h) plane allowed by the XENON100 limits [32] on $\sigma_{\text{DM-N}}$. In the left panel the low m_φ region is magnified to illustrate the two allowed bands. The one corresponding to the resonance region $m_h \sim 2m_\varphi$ (see also Fig. 7); for these values the annihilation is amplified to such an extent that (6.11) requires a very small coupling λ_x so that this region is allowed by the direct detection. Since the XENON100 data is available for $m_\varphi \geq 5$ GeV therefore the vertical band of masses below 5 GeV is also allowed. The right panel shows the large allowed area available for increasing m_{DM} where the sensitivity of XENON100 is reduced.

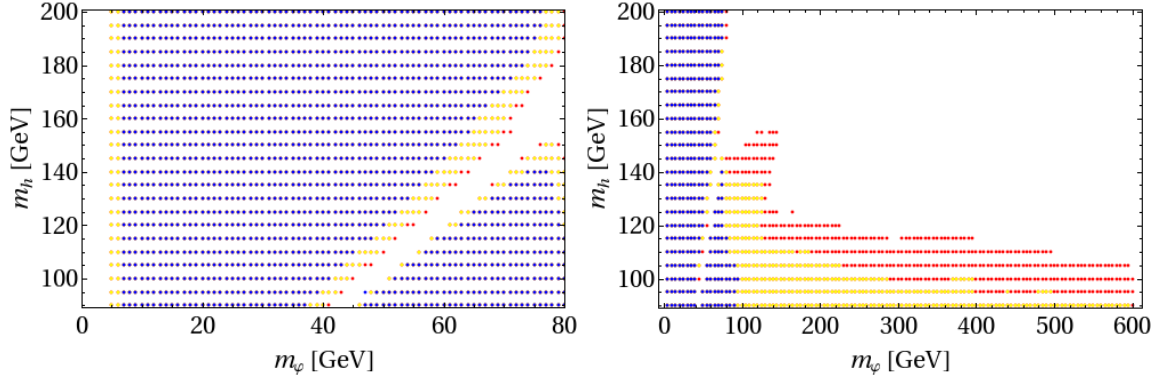


Figure 11. Constraint coming from the Xenon100 direct detection experiment combined with dark matter abundance in the case of CDM. Region forbidden for $N = 1$ is marked blue, for $N = 6$ blue and yellow, and $N = 12$ yellow, blue and red. The left panel magnifies the region of low scalar mass $m_\varphi < 80$ GeV, while the right one extends the mass range up to 600 GeV.

Recently a positive result for a direct detection in elastic scattering of DM particles off nucleons was announced [19] by the CRESST-II collaboration; with two points selected by a maximum likelihood fit (Tab. 4 and Fig. 8 in [19]) $M1 : \{m_{\text{DM}} = 25.3 \text{ GeV}, \sigma_{\text{DM-N}} = 11.6 \cdot 10^{-6} \text{ pb}\}$ and $M2 : \{m_{\text{DM}} = 11.6 \text{ GeV}, \sigma_{\text{DM-N}} = 3.7 \cdot 10^{-5} \text{ pb}\}$. These cross sections

are far above lower limit from XENON100 experiment [32], an issue that is yet to be resolved. As a complement to the implications derived above using the XENON100 limits, we will also discuss the consequences the CRESST-II results would have in constraining our model.

For each choice of m_h and N the requirement (6.11) determines a narrow allowed band in the (λ_x, m_φ) plane; an example is provided in Fig. 7 for the CDM case with $m_h = 130$ GeV and $N = 1, 6, 12$. It is natural to ask whether there exist m_h (in the region allowed by the present data) and N such that the corresponding band contains the most likely points $M1$ and $M2$ found by CRESST-II. The answer is contained in the top panels of Fig. 12, where the regions preferred by CRESST-II (within 2σ) are superimposed with predictions of our model for $N = 1, 2$ and $m_h = 110 - 140$ GeV when satisfying (6.11) at the 3σ level. As it is seen from the figure both regions are consistent with the model. For larger values of N our model is consistent only with the 2σ $M1$ contour for $m_\varphi \sim 50$ GeV. If confirmed, these data would provide a strong restriction on the scenario discussed in this paper; in particular a tightening of the allowed regions around the current central values would require $N \lesssim 5$. Moreover it has immediate and dramatic consequences for Higgs boson searches at Tevatron or LHC since the invisible $h \rightarrow \tilde{\varphi}\tilde{\varphi}$ decay has a substantial branching ratio for the parameter regions consistent with $M1$ or $M2$. This is illustrated in the middle and bottom panels of Fig. 12, where the branching ratio is plotted against scalar mass m_φ .

When $\lambda_x < 0$, the constraint (3.3) generates no restrictions and the branching ratio can be very large, $BR_{h \rightarrow \tilde{\varphi}\tilde{\varphi}} \sim 1$ (see middle panels of Figs. 12 and 13). In these figures we also plot maximum value of $BR_{h \rightarrow \tilde{\varphi}\tilde{\varphi}}$ calculated for $|\lambda_x|$ that saturates the vacuum stability bound (3.1) on $|\lambda_x|$ for a given quartic $\tilde{\varphi}$ self coupling $\lambda_\varphi = 8\pi, 1, 0.5$ and 0.1 , when $m_h = 130$ GeV; the regions above corresponding dashed curves are excluded by this constraint.

For $\lambda_x > 0$ the constraint (3.3) is important and excludes the region above the dotted curve shown in the bottom panels of Fig. 12 and 13. Within the allowed region the $BR_{h \rightarrow \tilde{\varphi}\tilde{\varphi}}$ is smaller, but it can still reach ~ 0.8 .

Note, that if one anticipates the cutoff Λ to be below $\sim 10^4$ GeV (as we do in this work) then the triviality upper limit for low N is roughly $\lambda_\varphi \lesssim 5$, so the branching ratio could easily reach even 99% without any conflict with triviality. It is also worth mentioning here that if $\lambda_x > 0$, then small value of m_φ in the $M1$ and $M2$ regions together with the consistency condition (3.3) imply $0.06 < \lambda_x < 0.24$, which is too small to ameliorate the SM fine tuning problem (see Sec. 5). On the other hand, if $\lambda_x < 0$, the vacuum stability bound (3.1) implies $|\lambda_x| < 0.85$ for $\lambda_\varphi \leq 8\pi$ and $110 \text{ GeV} < m_h < 141 \text{ GeV}$; then, as seen from Fig. 5, the allowed values for the cutoff Λ are smaller than for the SM. Therefore $\lambda_x < 0$ does not help solving the hierarchy problem regardless of the cosmological constraints.

From the top panels of Figs. 12 and 13 one observes that for $1 \leq N \leq 12$ low Higgs boson masses ($m_h = 110 - 120$ GeV) are preferred by the $M1$ region of heavier $\tilde{\varphi}$ (larger N favors smaller m_h). For the region of lighter m_φ ($M2$) roughly all Higgs boson masses fit data equally well, however only for $N = 1$ and 2 .

In conclusion, the CRESST-II positive result, if confirmed, would imply (within the

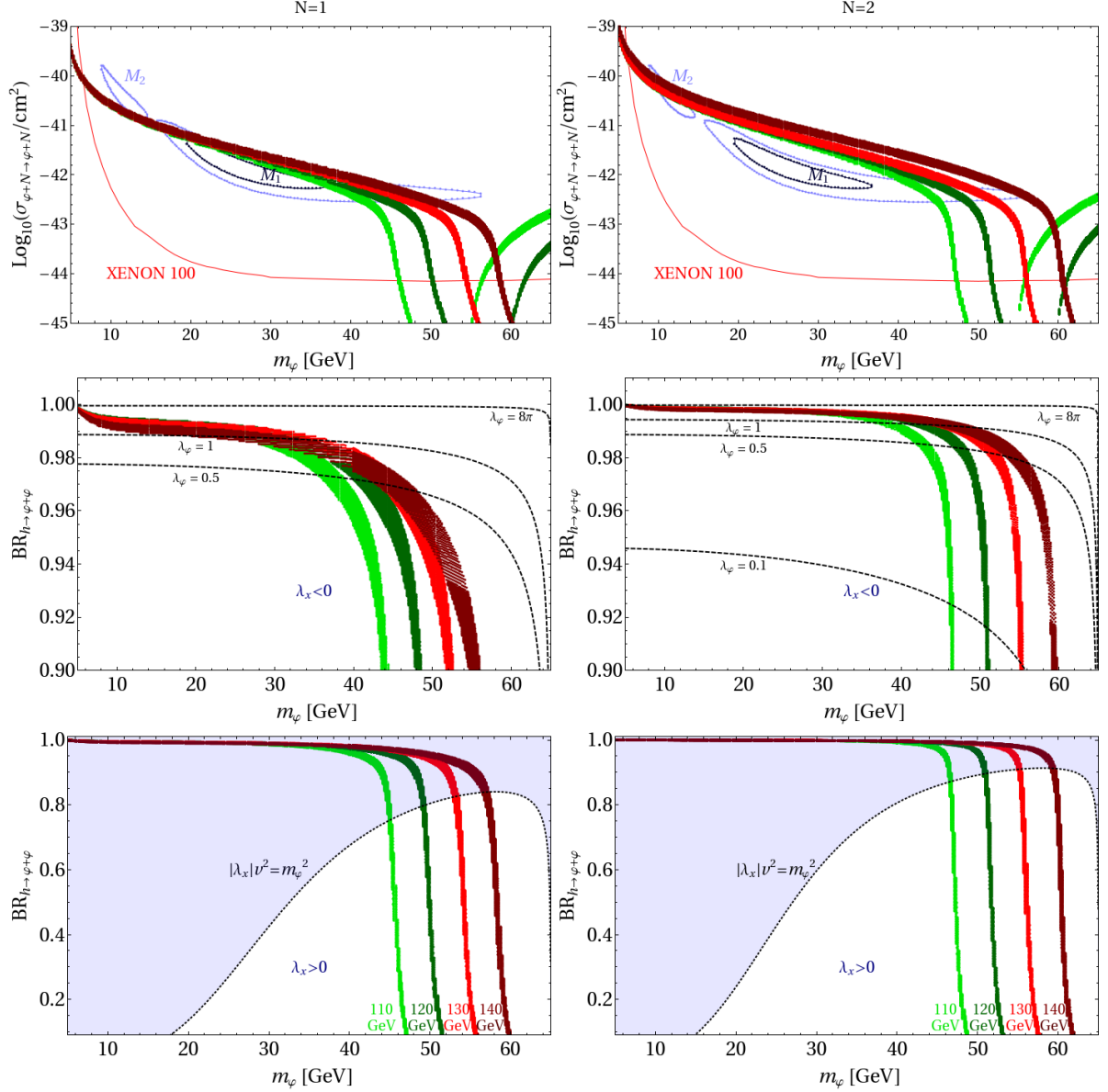


Figure 12. Top panels: singlet-nucleon cross section for $N = 1, 2$ as a function of m_φ when (6.11) is obeyed, the color bands correspond $m_h = 110$ GeV (green), 120 GeV (dark green), 130 GeV (red), 140 GeV (dark red); also shown the regions M1 and M2 favored by the CRESST-II experiment [19] at 1 and 2 σ level (black and blue closed curves, respectively), and the XENON100 limit [32]. Middle panels: the branching ratio $\text{BR}_{h \rightarrow \varphi\varphi}$ for $N = 1, 2$ as a function of m_φ , when $\lambda_x < 0$, for four values of m_h (color coded as above); the dashed lines show the value of $\text{BR}_{h \rightarrow \varphi\varphi}$ when λ_x saturates the stability bound (3.1) when the quartic φ^4 self coupling equals $\lambda_\varphi = 8\pi, 1, 0.5$ and 0.1 and for $m_h = 130$ GeV: regions consistent with both (6.11) and (3.1) lies on the colored bands and below the dashed curves. Lower panels: the branching ratio $\text{BR}_{h \rightarrow \varphi\varphi}$ for $N = 1, 2$ as a function of m_φ , when $\lambda_x > 0$, and for four values of m_h (color coded as above); the dotted line show the value of $\text{BR}_{h \rightarrow \varphi\varphi}$ when λ_x saturates the consistency bound (3.3): regions consistent with both (6.11) and (3.3) lie on the colored bands below the dotted line.

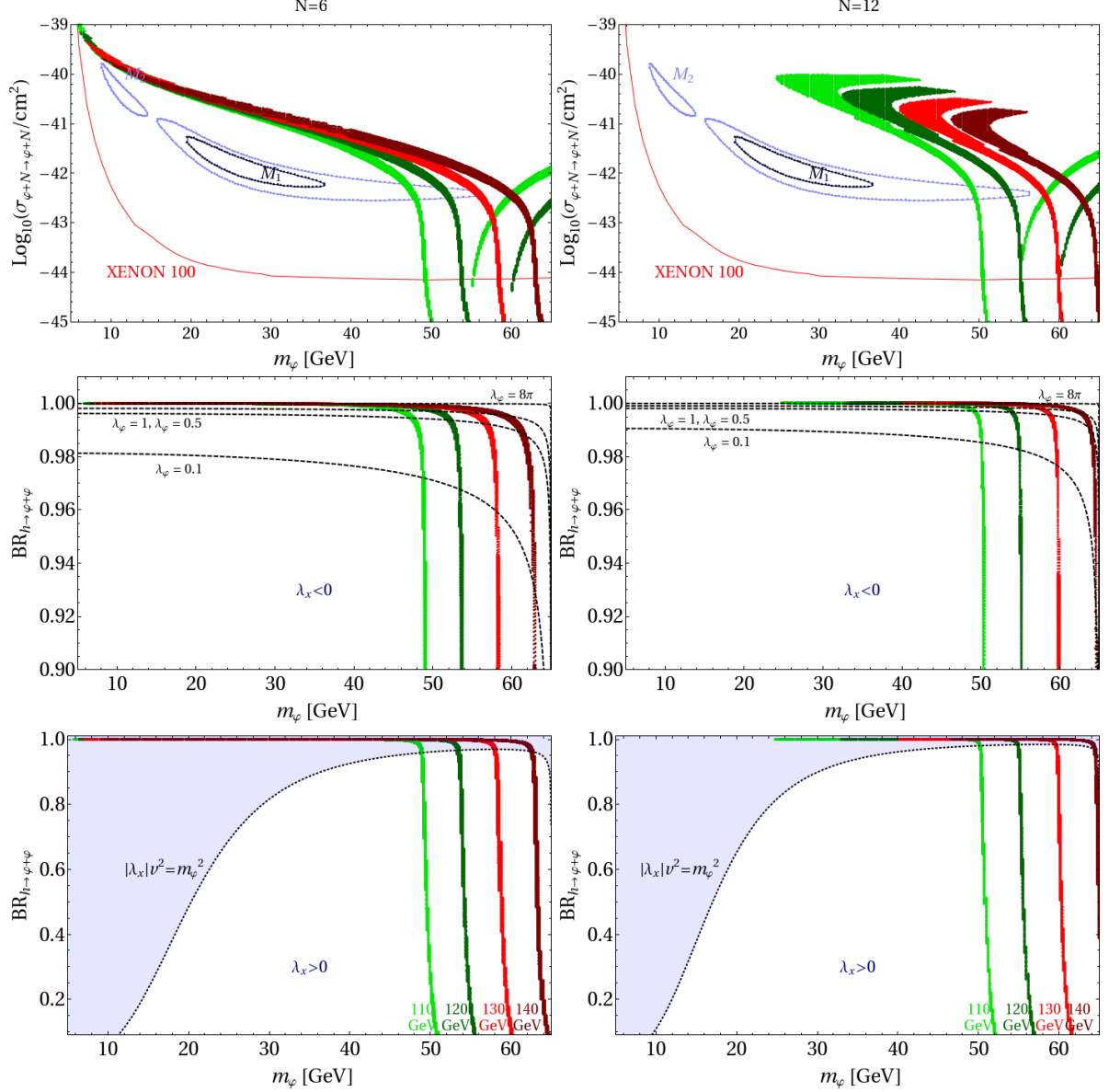


Figure 13. Similar as in Fig. 12, for $N = 6$ and $N = 12$.

singlet extension of the SM) that the Higgs boson could decay mainly invisibly, escaping discovery at both Tevatron and LHC. The option of invisibly decaying Higgs boson have been considered previously in [33].

8 Self-interacting DM

In spite of its many successes, the standard CDM cosmological model is also facing some difficulties when compared with recent observations. For instance, high-resolution N-body simulations have shown that the model generates a cusps in the DM density distribution in central regions of galaxies [34]. Another discrepancy concerns the number of subhalos

predicted by the model, which is at least factor of ten larger than the observed [35] number. Self-interacting DM was proposed by Spergel & Steinhardt [36] to cure these problems. Within this model, dark matter particles experience weak, non-dissipative collisions on scales of kpc to Mpc for typical galactic densities. This effect then generates a soft core in the inner regions of the dark halos, and it also ameliorates the overabundance of subhalos. The key requirement is that the mean free path of DM particles should be between 1 kpc and 1 Mpc in regions where the dark matter density is about $0.4 \text{ GeV}/\text{cm}^3$. This model has attracted much attention [37].

In order to discuss this idea quantitatively we define the elastic scattering cross section per unit mass for DM consisting of N species. We then imagine a clump of DM particles scattering off another such clump:

$$\frac{\sigma_{DM}}{m_{DM}} = \frac{\sum_{i=1}^N n_i \sum_{j,k,l}^N \sigma_{ij \rightarrow kl}}{\sum_{i=1}^N n_i m_i} \quad (8.1)$$

where i, j , etc. label the DM flavor (in our case, the components of $\vec{\varphi}$), m_i denote the corresponding masses, n_i the number density of i -th particles in the clump, and $\sigma_{ij \rightarrow kl}$ the 2 on 2 cross sections. Because of the $O(N)$ symmetry the $n_i = n$ and $m_i = m_\varphi$ are flavor-independent, therefore

$$\frac{\sigma_{DM}}{m_{DM}} = \frac{N \sum_{j,k,l}^N \sigma_{1j \rightarrow kl}}{N m_\varphi} = \frac{\sigma_{11 \rightarrow 11} + (N-1)\sigma_{11 \rightarrow 22} + (N-1)\sigma_{12 \rightarrow 12}}{m_\varphi} \quad (8.2)$$

We will define an auxiliary self-interaction cross section:

$$\sigma_{\vec{\varphi}\vec{\varphi}}(\lambda_1, \lambda_2, \lambda_3) = \frac{(m_h^4 \lambda_1 + 32m_\varphi^2 v^2 \lambda_3^2 - 4m_h^2 (m_\varphi^2 \lambda_1 + v^2 \lambda_2^2 + 2v^2 \lambda_3^2))^2}{128\pi m_\varphi^2 m_h^4 (m_h^2 - 4m_\varphi^2)^2} \quad (8.3)$$

where λ_1 is the coupling of the direct quartic interaction, λ_2 is the s-channel Higgs exchange coupling and λ_3 corresponds to the t- and u-channel Higgs exchange. Now the relevant cross sections are:

$$\sigma_{11 \rightarrow 11} = \sigma_{\vec{\varphi}\vec{\varphi}}(\lambda_\varphi, \lambda_x, \lambda_x) \quad (8.4)$$

$$\sigma_{11 \rightarrow 22} = \sigma_{\vec{\varphi}\vec{\varphi}}\left(\frac{\lambda_\varphi}{3}, \lambda_x, 0\right) \quad (8.5)$$

$$\sigma_{12 \rightarrow 12} = 2 \sigma_{\vec{\varphi}\vec{\varphi}}\left(\frac{\lambda_\varphi}{3}, 0, \lambda_x\right) \quad (8.6)$$

where the factor $\frac{1}{3}$ in (8.6) and (8.5) comes from the combinatorics of the relevant diagrams and the factor of 2 in (8.6) corresponds to the absence of two identical particles in the final state. The relevant diagrams are shown in Fig. 14.

In terms of the cross section per unit mass (8.2), the Spergel & Steinhardt hypothesis requires that

$$2.05 \cdot 10^3 \text{ GeV}^{-3} \lesssim \frac{\sigma_{DM}}{m_{DM}} \lesssim 2.57 \cdot 10^4 \text{ GeV}^{-3} \quad (8.7)$$

In this section we will investigate whether this constraint is consistent with all the other restrictions that we have imposed on the multi-singlet extension of the SM.

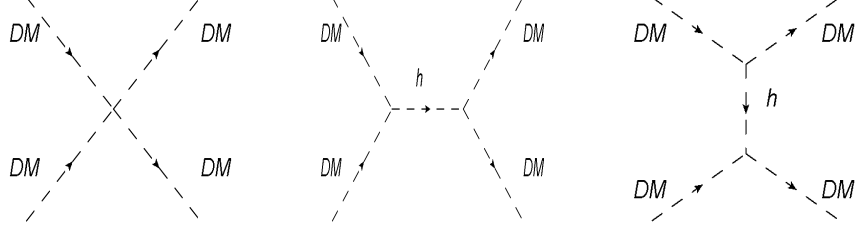


Figure 14. Feynman diagrams contributing to the elastic $\vec{\varphi}\vec{\varphi}$ scattering.

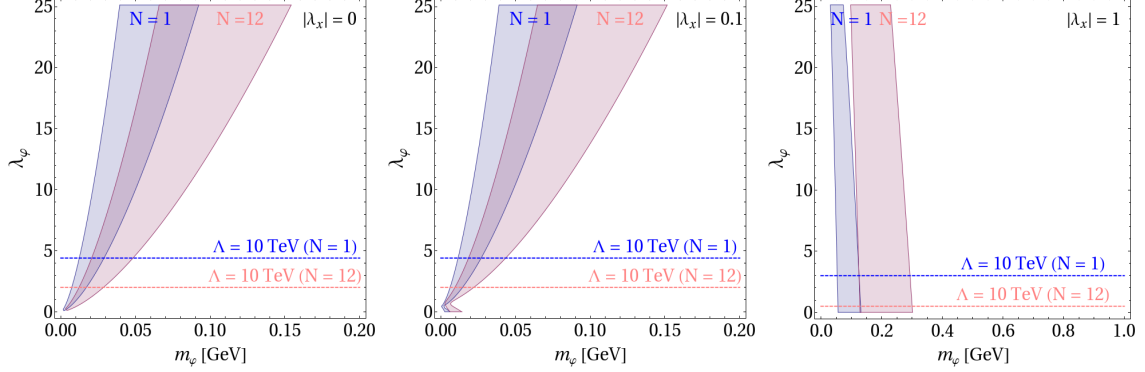


Figure 15. Regions in $(\lambda_\varphi, m_\varphi)$ space allowed by the Steinhard-Spergel hypothesis for $N = 1$ (blue/darker), $N = 12$ (pink/brighter) region and the Higgs-boson mass fixed at $m_h = 130$ GeV. The left, middle, and right panels correspond to $\lambda_x = 0, 0.1$ and 1.0 , respectively. The horizontal lines shows upper limits on λ_φ allowed by the triviality condition for the cutoff $\Lambda = 10$ TeV and $N = 1, 12$.

For a given N and m_h , the condition (8.7) defines an allowed region in $(\lambda_x, \lambda_\varphi, m_\varphi)$ space; the projections onto the $(m_\varphi, \lambda_\varphi)$ plane for fixed $|\lambda_x| = 0, 0.1, 1$ with $N = 1, 12$ and $m_h = 130$ GeV, are shown in Fig. 15. In the plots λ_φ varies from 0 up to 8π , the maximum value allowed by perturbative unitarity (3.2). It is clear that the condition (8.7) poses a very strong constraint on m_φ , which is restricted to small values, generally well below 1 GeV for $|\lambda_x| \lesssim 1$ and $N \lesssim 10$ (m_φ values ~ 100 GeV are allowed only for $|\lambda_x| \sim 10$ and $N \gtrsim 100$); similar results were obtained in other versions of scalar DM models [6, 31, 38].

If, in addition, one requires that the scale of physics beyond the singlet extension is above 10 TeV, then Landau poles are forbidden below this value for Λ ⁴. As a consequence, the limits on m_φ are much stronger, for example in the case of $\lambda_x = 0$ we obtain: $m_\varphi \lesssim 0.025$ GeV ($N = 1$) or $m_\varphi < 0.045$ GeV ($N = 12$).

As observed from Fig. 7 the values of m_φ that are required by the Spergel & Steinhardt condition (8.7) are not compatible with the CDM case. The only viable option is the FIDM. In this case, from Fig. 9 one can see that $m_\varphi \sim 0.01 - 0.05$ GeV corresponds to

⁴In our derivation of σ_{DM} we neglected radiative corrections: because of the small allowed values of m_φ , we expect that the effects from the renormalization group evolution of the couplings will be small, and for this reason in this section we do not differentiate between λ_φ and its initial value (4.6).

$\lambda_x \sim 10^{-10} - 10^{-12}$ for $N = 1 - 12$, and only the first panel in Fig. 15 is consistent with the DM abundance. Thus, within our model, the Spergel & Steinhardt hypothesis is consistent only with very light DM particles ($m_\varphi \lesssim 0.01 - 0.05$ GeV) that are very weakly coupled to the SM ($\lambda_x \sim 10^{-12} - 10^{-10}$).

9 Summary and conclusions

We have considered an extension of the Standard Model that contains a set of N real scalar gauge singlets $\vec{\varphi}$ that transform as the fundamental representation of a global $O(N)$ symmetry, under which all SM particles are singlets. This global symmetry remains unbroken, so that $\vec{\varphi}$ is a stable candidate for Dark Matter. The constraints on the model parameters implied by tree-level vacuum stability, unitarity and triviality were discussed. We have also investigated to what extent the presence of extra scalars could ameliorate the fine tuning of quadratic corrections to the Higgs boson mass.

The restrictions imposed by abundance of DM were also presented; in particular we showed that the recent CRESST-II data for DM-nucleus scattering, if confirmed, would imply that for this model the standard Higgs boson decays predominantly into pairs of Dark Matter scalars. In that case discovery of the Higgs boson at LHC and Tevatron is impossible. For $N = 1$ the most likely mass of the dark scalars lies in the range $15 \text{ GeV} \lesssim m_\varphi \lesssim 50 \text{ GeV}$ and $BR(h \rightarrow \vec{\varphi}\vec{\varphi}) \sim 96\%$. If $N \gtrsim 2$, the scalars have to be heavier: $50 \text{ GeV} \lesssim m_\varphi \lesssim 60 \text{ GeV}$, and $BR(h \rightarrow \vec{\varphi}\vec{\varphi}) \sim 98\%$. We have also shown that the Spergel-Steinhardt solution of the Dark Matter density cusp problem restricts the parameters to a Feebly Interacting Dark Matter region with $\lambda_x \sim 10^{-12} - 10^{-10}$ and scalar masses in the range $m_\varphi \sim 0.01 - 0.05$ GeV.

Acknowledgments

This work has been partially financed by the National Science Centre (Poland) as a research project, decision no DEC-2011/01/B/ST2/00438; and by the U. S. Department of Energy under Grant No. DEAC02-06CH11357. The authors thank both the XENON and CRESST-II collaborations for providing relevant data concerning the allowed regions in the $(\sigma_{DMN \rightarrow DMN}, m_{DM})$ space that were adopted for plots shown in this work. AD acknowledges financial support from the project "International PhD Studies in Fundamental Problems of Quantum Gravity and Quantum Field Theory" of Foundation for Polish Science, co-financed from the program IE OP 2007-2013 within European Regional Development Fund.

References

- [1] N. Jarosik, C. L. Bennett, J. Dunkley, B. Gold, M. R. Greason, M. Halpern, R. S. Hill, G. Hinshaw *et al.*, *Astrophys. J. Suppl.* **192**, 14 (2011). [arXiv:1001.4744 [astro-ph.CO]].

- [2] M. J. G. Veltman, F. J. Yndurain, Nucl. Phys. **B325**, 1 (1989).
- [3] V. Silveira, A. Zee, Phys. Lett. **B161**, 136 (1985).
- [4] J. McDonald, Phys. Rev. **D50**, 3637-3649 (1994). [hep-ph/0702143 [HEP-PH]].
- [5] C. P. Burgess, M. Pospelov, T. ter Veldhuis, Nucl. Phys. **B619**, 709-728 (2001). [hep-ph/0011335].
- [6] M. C. Bento, O. Bertolami, R. Rosenfeld, Phys. Lett. **B518**, 276-281 (2001). [hep-ph/0103340].
- [7] H. Davoudiasl, R. Kitano, T. Li, H. Murayama, Phys. Lett. **B609**, 117-123 (2005). [hep-ph/0405097].
- [8] J. J. van der Bij, Phys. Lett. **B636**, 56-59 (2006). [hep-ph/0603082].
- [9] X. -G. He, T. Li, X. -Q. Li, J. Tandean, H. -C. Tsai, Phys. Lett. **B688**, 332-336 (2010). [arXiv:0912.4722 [hep-ph]].
- [10] W. -L. Guo, Y. -L. Wu, JHEP **1010**, 083 (2010). [arXiv:1006.2518 [hep-ph]].
- [11] Y. Cai, X. G. He and B. Ren, Phys. Rev. D **83** (2011) 083524 [arXiv:1102.1522 [hep-ph]].
- [12] L. J. Hall and Y. Nomura, JHEP **1003**, 076 (2010) [arXiv:0910.2235 [hep-ph]].
- [13] A. Bandyopadhyay, S. Chakraborty, A. Ghosal, D. Majumdar, JHEP **1011**, 065 (2010). [arXiv:1003.0809 [hep-ph]].
- [14] C. E. Yaguna, JHEP **1108**, 060 (2011). [arXiv:1105.1654 [hep-ph]].
- [15] M. Pospelov and A. Ritz, arXiv:1109.4872 [hep-ph].
- [16] B. Grzadkowski, J. Wudka, Phys. Rev. Lett. **103**, 091802 (2009). [arXiv:0902.0628 [hep-ph]]; Acta Phys. Polon. **B40**, 3007-3014 (2009). [arXiv:0910.4829 [hep-ph]]; J. Phys. Conf. Ser. **259**, 012095 (2010).
- [17] A. Kundu, S. Raychaudhuri, Phys. Rev. **D53**, 4042-4048 (1996). [hep-ph/9410291].
- [18] C. F. Kolda, H. Murayama, JHEP **0007**, 035 (2000). [hep-ph/0003170]; J. A. Casas, J. R. Espinosa, I. Hidalgo, JHEP **0411**, 057 (2004). [hep-ph/0410298].
- [19] G. Angloher, M. Bauer, I. Bavykina, A. Bento, C. Bucci, C. Ciemniak, G. Deuter, F. von Feilitzsch *et al.*, [arXiv:1109.0702 [astro-ph.CO]].
- [20] B. W. Lee, C. Quigg, H. B. Thacker, Phys. Rev. **D16**, 1519 (1977).
- [21] G. Cynolter, E. Lendvai, G. Pocsik, Acta Phys. Polon. **B36**, 827-832 (2005). [hep-ph/0410102]; M. Gonderinger, Y. Li, H. Patel, M. J. Ramsey-Musolf, JHEP **1001**, 053 (2010). [arXiv:0910.3167 [hep-ph]].
- [22] M. J. G. Veltman, Acta Phys. Polon. **B12**, 437 (1981).
- [23] M. B. Einhorn, D. R. T. Jones, Phys. Rev. **D46**, 5206-5208 (1992).
- [24] Aleksandra Drozd, MSc Thesis 2010.
- [25] The ATLAS and CMS Collaborations, ATLAS-CONF-2011-157, CMS PAS HIG-11-023
- [26] K. Nakamura *et al.* [Particle Data Group Collaboration], J. Phys. G **G37**, 075021 (2010).
- [27] E. Kolb, M. Turner, *The Early Universe*, 1994
- [28] P. Gondolo, G. Gelmini, Nucl. Phys. **B360**, 145-179 (1991).

- [29] G. Bertone, (ed.), Cambridge, UK: Univ. Pr. (2010) 738 p
- [30] G. Belanger, F. Boudjema, A. Pukhov, A. Semenov, Comput. Phys. Commun. **180**, 747-767 (2009). [arXiv:0803.2360 [hep-ph]].
- [31] J. McDonald, Phys. Rev. Lett. **88**, 091304 (2002). [hep-ph/0106249].
- [32] E. Aprile *et al.* [XENON100 Collaboration], arXiv:1104.2549 [astro-ph.CO].
- [33] T. Binnoth, J. J. van der Bij, Z. Phys. **C75**, 17-25 (1997). [arXiv:hep-ph/9608245 [hep-ph]]; R. Akhoury, J. J. van der Bij, H. Wang, Eur. Phys. J. **C20**, 497-505 (2001). [hep-ph/0010187].
- [34] J. F. Navarro, C. S. Frenk, S. D. M. White, Astrophys. J. **490**, 493-508 (1997). [astro-ph/9611107].
- [35] A. A. Klypin, A. V. Kravtsov, O. Valenzuela, F. Prada, Astrophys. J. **522**, 82-92 (1999). [astro-ph/9901240].
- [36] D. N. Spergel, P. J. Steinhardt, Phys. Rev. Lett. **84**, 3760-3763 (2000). [astro-ph/9909386].
- [37] B. D. Wandelt, R. Dave, G. R. Farrar, P. C. McGuire, D. N. Spergel, P. J. Steinhardt, [astro-ph/0006344].
- [38] D. E. Holz, A. Zee, Phys. Lett. **B517**, 239-242 (2001). [hep-ph/0105284].